

E. Paul McClain
National Environmental Satellite, Data, and Information Service, NOAA
Federal Building 4, Washington, DC 20233, USA

ABSTRACT

Visual and infrared measurements from the five-channel AVHRR on the NOAA-7 satellite are used operationally to derive sea surface temperatures. The multi-channel data are used to perform daytime and nighttime cloud-detection tests, and the several atmospheric-window channels in the thermal infrared are used to correct for atmospheric attenuation. Monitoring of the sea surface temperature product with buoy data indicates stability in mean bias ($\leq +0.1^\circ\text{C}$) and rms difference (0.6-0.8 $^\circ\text{C}$.) with little variation by season or geographic area. Global mapping enables the derivation of monthly mean isotherms, monthly and annual changes, and anomaly patterns relative to climatology. Problems have been associated with noise in the 3.7 μm window channel, and with the injection of substantial volcanic aerosol into the stratosphere by the El Chichón eruption. Multi-channel sea surface temperature charts are used in studies of such phenomena as equatorial long waves and the recent El Niño episode.

1. INTRODUCTION

Sea surface temperature fields on several spatial and temporal scales are of considerable interest to oceanographers, meteorologists, and climatologists. The irregular distribution and often variable quality of conventional intake temperatures from commercial ships, and the paucity of higher quality XBT and buoy observations, has stimulated interest in the repetitive and comprehensive coverage afforded by Earth-orbiting spacecraft.

Routine processing of infrared (IR) data from the NOAA series polar orbiting environmental satellites for global distributions of sea surface temperature (SST) began late in 1972 (Brower et al., 1976). Although the radiometers at that time performed their primary task of nighttime cloud imaging satisfactorily, the IR measurements were rather noisy and thus cloud-filtering was cumbersome and not as effective as required for extraction of SSTs. Furthermore, the single atmospheric "window" channel in the thermal-IR part of the spectrum did not permit adequate correction for atmospheric attenuation, chiefly by water vapor, which is very appreciable in tropical regions. Subsequent attempts to improve upon both cloud detection and atmospheric corrections by incorporating data from atmospheric sounders aboard the spacecraft were only partially successful (Walton et al., 1976). Although still based on IR measurements from a single window channel, higher-resolution, lower noise-level radiometric data from the Advanced Very High Resolution Radiometer (AVHRR) on the TIROS-N generation of NOAA operational satellites (Schwalb, 1978), together with better sounder measurements, enabled further improvements in SSTs (Walton, 1980).

Electrical interference in the 3.7 μm window channel of the first AVHRR (on TIROS-N) hindered early development and implementation of multiple-window techniques, but simulations and preliminary testing with measurements from the second AVHRR (on NOAA-6) were quite encouraging (McClain, 1980). The third AVHRR (on NOAA-7) has

three IR window channels, and operational processing of multi-channel SST (MCSST) commenced in November of 1981 (McClain et al., 1983).

This paper will give brief discussions of NOAA's MCSST processing, validation of MCSSTs, some global and regional products, and recent improvement activities. Use of MCSST analyses in atmospheric/oceanographic research, and some gaps in our knowledge or understanding, will be addressed.

2. DESCRIPTION OF MULTICHANNEL SST (MCSST) METHOD

Spatial resolution of the AVHRR at nadir is 1.1 km locally and nominally 4 km regionally and globally. Measurements are made in the visual (0.58-0.68 μ m), reflected IR (0.725-1.1 μ m), and in three emitted-IR windows (3.55-3.93, 10.3-11.3, and 11.5-12.5 μ m). Each orbital swath is about 2500 km wide on the Earth and each geographic area is viewed near 0300 and 1500 local time. Only the IR channels have provision for onboard calibration.

2.1 Cloud Detection Tests

Bi-directional reflectance measurements from the visual or reflected-IR channels are primary in the daytime cloud tests. Visible cloud threshold tests take advantage of the ocean/atmosphere reflectance being very low in the absence of clouds or glitter (specular reflectance). These Thresholds have been determined as a function of solar zenith angle, satellite zenith angle, and azimuth of the viewed spot. When clouds partially fill a scanspot of the radiometer, reflectances from neighboring scanspots will generally differ by more than the low noise level of the measurements. This provides the basis for an additional test, essentially requiring spatial uniformity. Because both visible threshold and visible uniformity tests can erroneously fail in glitter-contaminated areas, the option exists to use the nighttime IR-uniformity test in the daytime as well.

Nighttime cloud tests, of necessity, are based on data from the thermal-IR channels of the AVHRR. Threshold tests utilize the highest and lowest historically observed ocean surface temperatures; and a spatial uniformity test takes advantage of the high spatial resolution and low noise levels of the IR data taken in conjunction with the expectation of low horizontal gradients in both the SST and atmospheric attenuation. These assumptions are satisfied in most ocean areas and meteorological situations, but can fail at times, usually in coastal areas. Although these are the primary tests, a special test is used to detect low-altitude stratus clouds with uniform cloud top temperatures and that fill the radiometer's field of view. The reflectivity of optically-thick water droplet clouds is significantly greater at 3.7 than at 11 μ m, and this has the effect of making the $T_{3.7}-T_{11}$ difference much more negative than under any cloud-free conditions (McClain et al., 1983). Two other final filters can be used at night to remove a small residue of cloud-contaminated cases. The first such test intercompares the MCSST values obtained from the dual-window, split-window, and triple-window equations (see next section), which have differing sensitivities to the presence of sub-resolution cloud contamination, and requires that they agree to within some limit, generally 0.5-1.0C. The second test requires that the triple-window MCSST not deviate markedly from the climatological SST (by more than 4-7°C, dependent on the climatological SST gradient).

2.2 Correction for Atmospheric Attenuation

Although the idea of using the different atmospheric transmittance characteristics of the several window regions in the infrared to devise an atmospheric attenuation correction scheme for satellite-derived SST goes back to at least Anding and Kauth (1970), the theoretical basis was explicated by Prabhakara et al. (1974)

and McMillin (1975), with the former being the first to verify the approach with radiometric measurements from space. A number of AVHRR simulations using model atmospheres and atmospheric transmittance models have been performed, among them Deschamps and Phulpin (1980), McClain (1981), and Barton (1983), and all found highly linear relations between the atmospheric correction and various combinations of channel brightness temperatures or brightness temperature differences, with standard errors of estimation generally falling in the 0.1-0.3°C range.

NOAA's operational MCSST equations from NOAA-7 were derived from the following simulation equations (°K in, °C out), which are based on a seasonally and geographically diverse set of 64 atmospheric soundings from marine areas of the world and atmospheric transmittance models (Weinreb & Hill, 1980):

$$T_{3/4} = T_{11} + 1.4887(T_{3.7} - T_{11}) - 271.85 \quad (\text{dual-window}) \quad (1)$$

$$T_{4/5} = T_{11} + 2.4917(T_{11} - T_{12}) - 273.48 \quad (\text{split-window}) \quad (2)$$

$$T_{3/4/5} = T_{11} + 0.95321(T_{3.7} - T_{12}) - 272.54 \quad (\text{triple-window}) \quad (3)$$

No explicit allowance for aerosol is incorporated in this set of equations, and the IR reflectance, the satellite zenith angle, and the sea-air temperature difference are all assumed to be zero.

3. VALIDATION OF MCSST RETRIEVALS

Initial testing of Eqn. (1) with NOAA-6 data (McClain, 1981) revealed temperature-dependent biases of up to 2°C and a root mean square (rms) difference of 1.1°C. A relatively small set of expendable bathythermograph (XBT) and moored buoy measurements was employed to define temperature-dependent bias corrections for initial incorporation in the several MCSST operational algorithms (McClain et al., 1983). More extensive sets of drifting buoy observations have been collected and matched to satellite measurements over diverse geographic areas and all seasons to determine the coefficients for the current operational equations (Strong and McClain, 1984), given below:

$$T_{4/5D} = 1.0346T_{11} + 2.58(T_{11} - T_{12}) - 283.21 \quad (\text{day}) \quad (4)$$

$$T_{3/4} = 1.0008T_{11} + 1.50(T_{3.7} - T_{11}) - 273.34 \quad (5)$$

$$T_{4/5N} = 1.0350T_{11} + 2.58(T_{11} - T_{12}) - 283.18 \quad (\text{night}) \quad (6)$$

$$T_{3/4/5} = 1.0170T_{11} + 0.97(T_{3.7} - T_{12}) - 276.58 \quad (7)$$

Validation of these equations with respect to independent satellite measurements and data from a totally different set of drifting buoys is given by the statistics in Table 1. It should be noted that although MCSST equations involving measurements from the 3.7µm channel can be used in the daytime, care must be taken to avoid sun glitter areas. Reflected solar radiation there elevates the brightness temperature above the value corresponding to emission alone.

Table 1. Validation of MCSSTs with respect to drifting buoy data

Equation	Split-window		Triple-window	Dual-window
	day	night	night	night
N	68	84	84	84
bias	-0.02	-0.08	-0.01	+0.02
rmsd	0.49	0.62	0.57	0.79

4. GLOBAL MAPPING OF MCSST

Using satellite zenith angles of up to 45°, 12 hourly global coverage of 4-km AVHRR scanspot data is used to process hundreds of thousands of 11x11 scanspot arrays, called targets, over the oceans daily. Cloud tests and atmospheric corrections are applied to 2x2 unit arrays (8x8 km) within the targets, targets being centered about every 25 km. Using the most centrally located (day) or the warmest (night) of the cloudfree unit arrays within the target, 15,000-20,000 daytime and about 20,000 nighttime MCSST retrievals are made each day over the globe. The less constrained daytime cloud tests allow observational densities of up to 25 retrievals per target as an option.

A variety of contoured MCSST fields is generated from the 8-km resolution retrievals, which are nominally spaced every 25 km or less depending on cloud distribution and daytime observational density mode. All the daily (daytime and nighttime) MCSST retrievals are composited onto weekly 100-km (global) and 50-km (regional) grids, and a 14-km grid for coastal areas is under testing. The search distance for each grid point is an inverse function of the SST gradient, being a maximum of 200 km for the 100-km grid. Each MCSST retrieval within the search area is weighted, the maximum weight being applied to those within 1/3 of a grid interval, and the weight decreasing with the square of the distance from there. The distance-weighted average retrievals for each grid point each day are composited into a weighted average for the week by further weighting each retrieval as an inverse function of its age.

The final weekly fields are contoured at 1°C intervals with the isotherms being dashed in areas where the grid-point MCSSTs have not been updated within the past seven days. Figure 1 is an example of a 50-km regional chart in the eastern equatorial area of the Pacific.

All MCSST retrievals for the month are collected and averaged in 2.5° latitude/longitude bins for purposes of generating fields of monthly means, departures from historical means, (i.e., anomalies), month-to-month and year-to-year changes, etc. Figure 2 is a portion of the monthly anomaly chart for September 1982 during the early stages of a recent El Niño episode.

5. MCSST IMPROVEMENTS

Although the basic bias-corrected MCSST algorithms have been performing adequately under most conditions, certain situations are in need of further study. Among these are corrections for very large satellite zenith angles, for very large sea/air temperature differences, and for severe aerosol conditions.

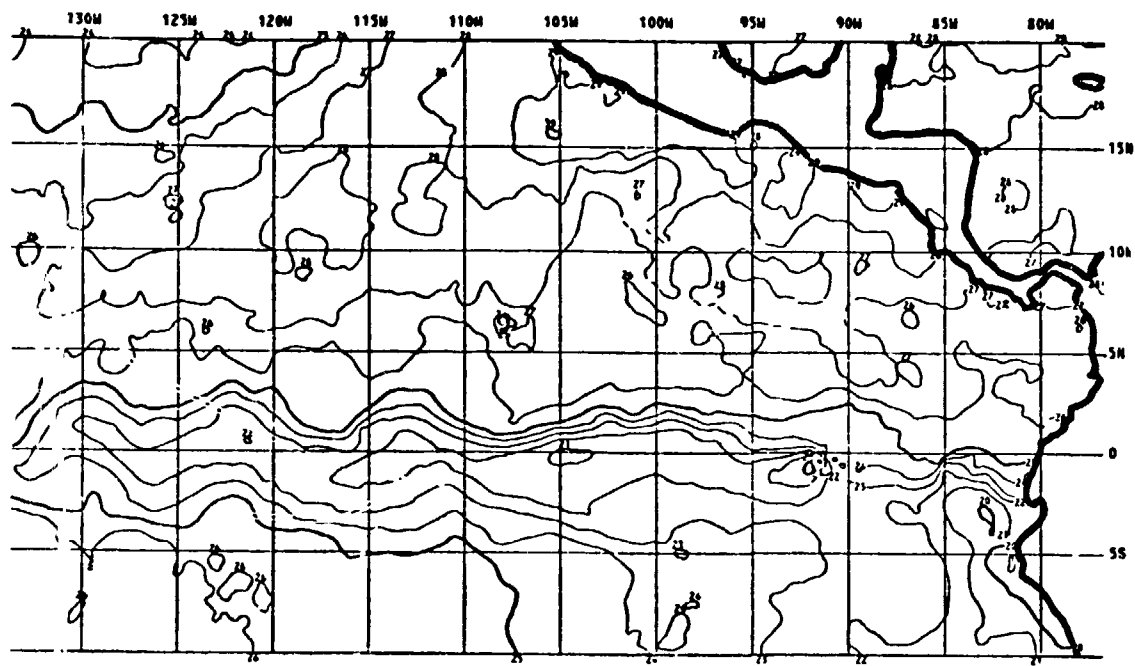


Figure 1. 50-km MCSST analysis, week ending Nov. 8, 1983, in eastern equatorial Pacific

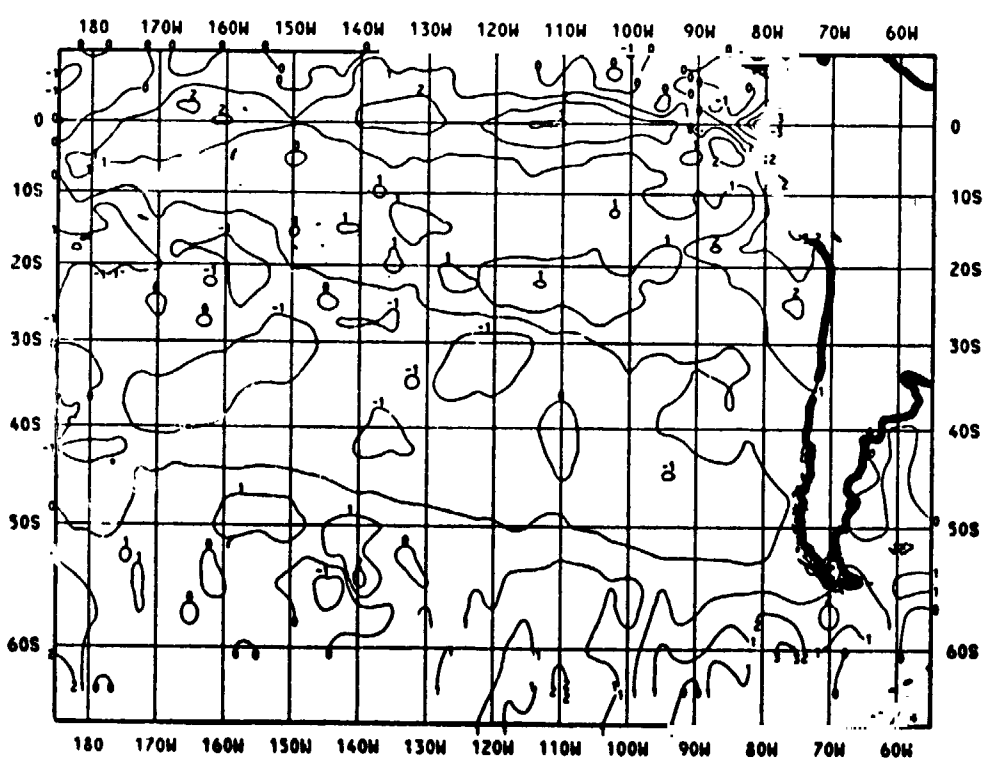


Figure 2. Portion of global MCSST monthly mean anomaly for September 1982

5.1 Large Satellite Zenith Angles

ORIGINAL PAGE IS
OF POOR QUALITY

Although the longer path length through water vapor at higher satellite zenith angles (sza) results in larger brightness temperature differences, and thus larger atmospheric corrections, it can be shown by simulation that this implicit compensation is inadequate when $\text{sza} > \sim 45^\circ$, particularly in the moistest atmospheres. Adding a term of the form $K(T_i - T_j)(\sec \theta - 1)$ where T_i and T_j are brightness temperatures in two of the window channels, θ is the sza, and K is a constant, enables improved corrections at sza values of $45\text{--}60^\circ$. Table 2 below compares the satellite minus buoy/XBT statistics for 22 daytime (eastern North Atlantic) and eight nighttime (Mediterranean) matchups in March 1982 using Eqn. (2) and the following NOAA/NESDIS split-window simulation equation (Llewellyn-Jones, 1983):

$$T_{4/5\text{sza}} = T_{11} + 2.346(T_{11} - T_{12}) + 0.655(T_{11} - T_{12})(\sec \theta - 1) - 273.30 \quad (8)$$

Table 2. Split-window MCSSTs with and without sza correction terms (Llewellyn-Jones, 1983)

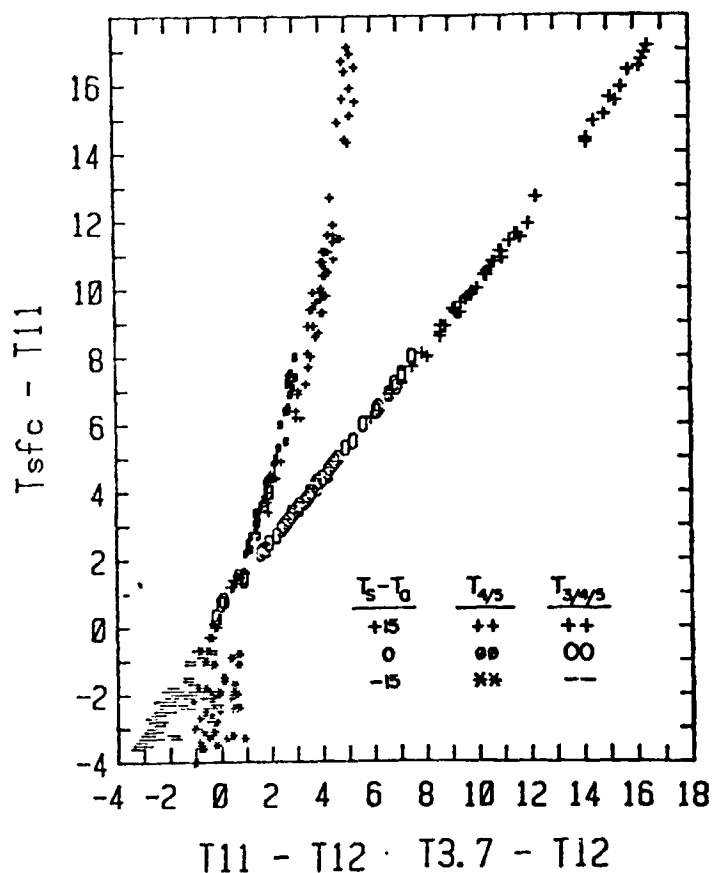
<u>Equation</u>	<u>N</u>	<u>bias</u>	<u>rmsd</u>
(2)	28	-0.44	0.67
(8)	28	-0.15	0.44

5.2 Large Sea/Air Temperature Differences

It can be demonstrated by simulation that sea/air temperature differences (sa Δ T) of to $5\text{--}10^\circ\text{C}$, particularly if positive (sea warmer), result in very little error in retrieved MCSST when the algorithms based on sa Δ T=0 are used. The very large negative sa Δ T values, however, that are common in some areas (e.g., the Great Lakes and just off the NE coast of the USA in late spring and early summer) are associated with significant errors when certain of the MCSST equations are used. It is clear from the split-window and triple-window simulations in Fig. 3 that the latter equation is the preferred one in such situations, although the usual care to avoid specular reflection (glitter) areas must be taken in the daytime. Table 3 gives the bias and rms differences when the surface temperature is predicted by Eqn. (3) or Eqn. (4) using simulation data sets corresponding to $T_s - T_a = -15, 0, \text{ and } +15^\circ\text{C}$.

Table 3. Simulations with MCSST equations assuming $T_s - T_a = 0$

<u>$T_s - T_a$</u>	<u>Split-window equation</u>			<u>Triple-window equation</u>		
	<u>N</u>	<u>bias</u>	<u>rmsd</u>	<u>N</u>	<u>bias</u>	<u>rmsd</u>
-15	67	+1.30	1.86	67	+1.04	1.10
0	67	+0.00	0.38	67	-0.01	0.07
+15	67	-0.63	1.76	67	-0.05	0.37



ORIGINAL PAGE IS
OF POOR QUALITY

Figure 3. Split-window ($T_{4/5}$) and triple-window ($T_{3/4/5}$) atmospheric corrections for simulated extreme sea-air temperature differences

5.3 Severe Aerosol Situations

The dust veil from the eruption of El Chichón in April 1982 had a severe impact on MCSST processing for over a year, especially in the band from about 0-30°N latitude (Strong et al., 1983). Not only were daytime MCSST cloud tests failed because of reflected radiation from the volcano cloud, but nighttime retrievals were characterized by substantial negative biases from increased attenuation by minute sulfuric acid droplets at very low temperatures. The Weinreb & Hill (1980) atmospheric transmittance models were used with a diverse set of 56 atmospheric soundings, with and without hypothesized El Chichón type aerosols, to determine simulated brightness temperatures for the AVHRR window channels. The left two graphs of Fig. 4 show the simulated triple-window relation between the attenuation temperature depression in T_{11} and the temperature difference ($T_{3.7} - T_{12}$). The aerosol-free data show the unique linear relation with extremely small scatter that is the basis of Eqn. (3) discussed in Sec. 2.2. The lower-left graph shows the same relation when two other aerosol concentrations are included, the 56 soundings being evenly divided into three aerosol classes. Each class exhibits a different relationship; i.e., no unique solution for SST appears. The graph at the right shows an alternative triple-window relationship, the temperature depression in T_{12} vs. $T_{3.7} - T_{11}$, but with the same aerosol classes as at lower left. Although the scatter is greater than in the aerosol-free case, there appears a unique relationship that is not sensitive to aerosol concentration. Preliminary testing of a volcano MCSST algorithm based on this result was encouraging, but extensive testing was precluded by a severe noise problems in the 3.7 μ m channel (see Sec. 7).

In addition, efforts are underway to extend the work of Griggs (1981) to severe aerosol conditions, and then to develop corrections to MCSSTs based on dynamic estimates of aerosol optical thickness from concurrent visual channel AVHRR data (Schwedfeger et al., 1983). Other extreme aerosol situations, such as Saharan dust outbreaks over the eastern subtropical Atlantic, also are known to affect certain MCSST retrievals, but investigations of these are just getting underway.

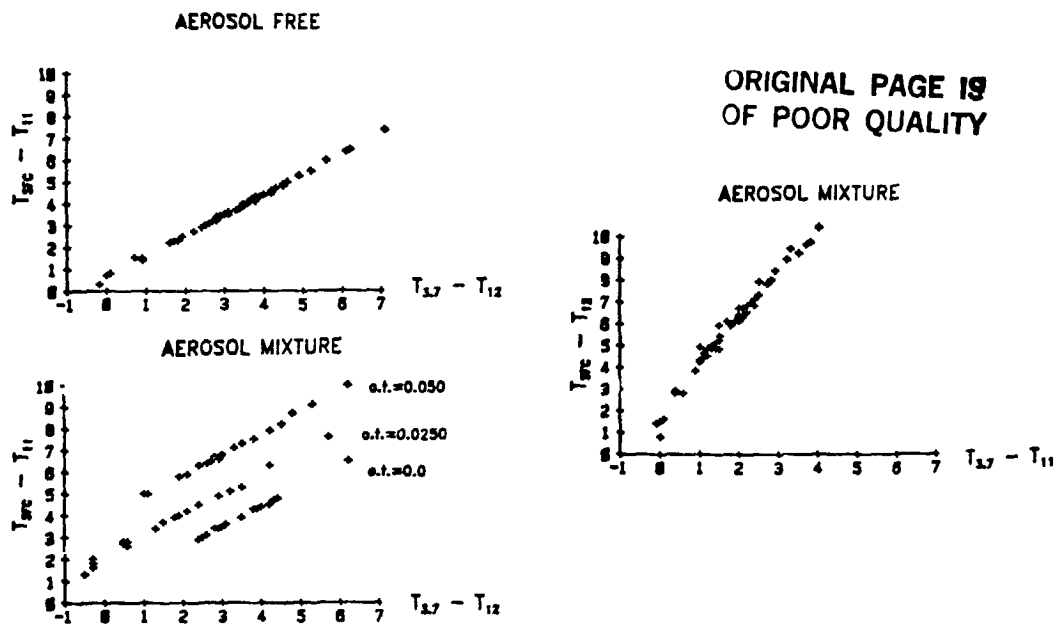


Figure 4. Multi-window atmospheric corrections for simulated volcanic aerosols

6. USE OF MCSSTs IN ATMOSPHERIC/OCEANIC RESEARCH

Although available operationally for just two years, and plagued during much of that time with El Chichon effects and noise problems in the 3.7 m data, MCSSTs are seeing increased use both operationally and in research. Legeckis' investigation of equatorial long waves in the eastern equatorial Pacific continues to be greatly aided by the regional 50-km charts (Legeckis et al., 1983). Some of these westward-moving waves are readily apparent in the isotherms in Fig. 1. The El Nino episode of 1982-83 was unusual in many respects (Rasmusson and Wallace, 1983), but among them was the intense positive SST anomaly that first began to develop along the equator between the Galapagos and the date line during the late summer of 1982. Few ships or other *in situ* observations were available in this area, especially during the early stages, and the MCSST analyses were the first operational charts to clearly depict the extent and amplitude of the anomalously warm water in that region (Strong, 1983). The anomaly as it was in September 1982 is seen in Fig. 2. MCSST techniques also were employed extensively by researchers involved in the Gulf Stream Rings Project (Brown, 1983).

7. CONCLUDING REMARKS

Although some of the physical processes are not really accounted for in the fairly simple theoretical models employed to date, especially those associated with high concentrations of aerosols, the effects of most are sufficiently small and/or compensating that their net effect on the MCSST is also rather small, thus accounting for the stability of the good area-wide and season-wide accuracies measured relative to drifting buoys. Similar matchup statistics have been obtained daily on a global basis as part of the MCSST operational processing with respect to intake temperatures from so-called ships of opportunity. The statistics against ships tend to be poorer and more variable than those against drifting huoyos (Strong and McClain, 1984), but this follows from the fact that ship SSTs matched with other ship SSTs (within 24 hours and 100 km) consistently have been found to have differences with a standard deviation of 1.5-2.0°C. There is the

possibility of increasing the accuracy of multi-window SSTs yet further by adding further by adding multiple viewing-angle capability. The results of simulations at the Rutherford Appleton Laboratory in England have been encouraging (Llewellyn-Jones, 1983), and this approach is incorporated in the design of the Along Track Scanning Radiometer proposed for the ERS-1 satellite.

A often asked question is the difference to be expected between the "skin temperature" sensed by a radiometer in space and a "bulk temperature" measured by an in situ sensor on a buoy (depth of 1 meter) or in a ships water-intake manifold (depth of perhaps 10 meters). This skin minus bulk temperature difference should be 0.2°C or less with well-mixed upper layers; but in the daytime under a high sun and very light winds, the skin temperature can easily be elevated several degrees above that at depth.

A recurring engineering problem has been electrical interference in the 3.7 μ m channel, the noise level increasing with time following launch of the spacecraft. The less severe noise levels can be compensated for in the MCSST processing (e.g., using larger unit arrays) at the consequent expense of lower observational densities and somewhat degraded accuracies from poorer cloud filtering. NOAA-7 noise levels had increased so much by June 1981 that it necessitated abandonment of this channel because of serious nighttime SST product degradation. Outgassing procedures were carried out on NOAA-7 for a week in September 1983, and this reduced the noise to very low levels again. Monitoring is being maintained to ascertain whether the noise returns and at what rate of increase.

Although serious attempts to map sea surface temperature globally from space have been underway since early in the 1970's, only since late in 1981 when multi-channel sea surface temperatures began to be processed operationally from AVHRR measurements, have the coverage and accuracy achieved levels where oceanographers and meteorologists alike are beginning to use satellite-derived SSTs in their activities. With good coverage provided by satellite-based sea surface temperatures in the Southern Hemisphere oceans and other data-sparse areas, a truly global time series becomes feasible.

8. ACKNOWLEDGEMENTS

The author acknowledges the important contribution of C. C. Walton to the subsection on severe aerosol situations, the assistance of A. E. Strong to the subsection on large sea/air temperature differences, and the help of O. L. Smith by typing of the manuscript.

9. REFERENCES

- Anding, D. and R. Kauth, 1970: Estimation of sea surface temperature from space. *Remote Sensing of Environ.*, 1, 217-220.
- Barton, I. J., 1983: Dual channel satellite measurements of sea surface temperature. *Quart. Jour. Roy. Met. Soc.*, 109, 365-378.
- Brower, R. L., H. D. Gohrband, W. G. Pichel, T. L. Signore, and C. C. Walton, 1976: Satellite derived sea surface temperatures from NOAA spacecraft. NOAA Tech. Memo. NESS 78, U.S. Dept. of Commerce, Wash., DC, 74 pp.
- Brown, O. B., 1983: personal communication. Rosenstiel School of Marine and Atmospheric Science, Univ. of Miami, Coral Gables, FL 33124.
- Deschamps, P. Y. and T. Phulpin, 1980: Atmospheric correction of infrared measurements of sea surface temperature using channels 3.7, 11, and 12 m. Boundary

Layer Meteor., 18, 131-143.

- Griggs, M., 1981: AVHRR measurements of atmospheric aerosol over oceans. Report, NOAA Contr. #MO-A01-78-0J-4092, Sci. Applic., Inc., LaJolla, CA., 50 pp.
- Legeckis, R., W. Pichel, and G. Nesterczuk, 1983: Equatorial long waves in geostationary satellite observations and in a multi-channel sea surface temperature analysis. *Bull. Am. Meteor. Soc.*, 64, 133-139.
- Llewellyn-Jones, D. T., 1983: in *Satellite-Derived Surface Temperature: Workshop II*. NASA/JPL, Pasadena, CA (in press).
- McClain, E. P., 1981: Multiple atmospheric-window techniques for satellite-derived sea surface temperatures. *Oceanography From Space* (J.F.R. Gower, Ed.). Plenum Press, New York, NY, 73-85.
- McClain, E. P., W. G. Pichel, C. C. Walton, Z. Ahmad, and J. Sutton, 1983: Multi-channel improvements of satellite-derived global sea surface temperatures. *Adv. Space Res.*, 2, 43-47.
- McMillin, L. M., 1975: Estimation of sea surface temperatures from two infrared window measurements with different absorption. *Jour. of Geophys. Res.*, 80, 5113-5117.
- NASA/JPL, 1983: *Satellite-Derived Surface Temperature: Workshop I*. JPL Publ. 83-34, Pasadena, CA, 147 pp.
- Prabhakara, C., G. Dalu, and V. G. Kunde, 1974: Estimation of sea surface temperature from remote sensing in the 11 to 13 μ m window region. *Jour. of Geophys. Res.*, 79, 5039-5044.
- Rasmusson, E. M. and J. M. Wallace, 1983: Meteorological aspects of the El Nino/Southern Oscillation. *Science*, 222, 1195-1202.
- Schwalb, A., 1978: The TIROS N/NOAA A-G satellite series. NOAA Tech. Memo. NESS 95, U.S. Dept. of Commerce, Wash., DC, 75 pp.
- Schwedfeger, A., L. L. Stowe, and A. Gruber, 1983: Sensitivity of Earth radiation budget parameters for El Chichon volcanic aerosol as estimated from NOAA-7 AVHRR data. Preprint 5th Conf. Atmos. Rad., Baltimore, MD. 3pp.
- Strong, A. E., 1983: El Nino observations by remote sensing. *Proceed. 17th Internat. Symp. on Remote Sens. Environ.*, Ann Arbor, MI, 177-184.
- Strong, A. E. and E. P. McClain, 1984: Improved ocean surface temperatures from space--comparisons with drifting buoys. *Bull. Am. Meteor. Soc.* (in press).
- Walton, C. C., R. L. Brower, and T. L. Sigmere, 1976: Satellite-derived sea surface temperatures by multi-channel regression. *Proceed. COSPAR Symp. on Meteor. Obs. from Space, COSPAR XIX*, Philadelphia, Pa., 8-10 June 1976, 155-159.
- Walton, C. C., 1980: *Deriving sea surface temperatures from TIROS-N data. Remote Sensing of Atmospheres and Oceans*, Academic Press, 547-579.
- Weinreb, M. P. and M. L. Hill, 1980: Calculations of atmospheric radiances and brightness temperatures in infrared window channels of satellite radiometers. NOAA Tech. Memo. NESS 80. U. S. Dept. of Commerce, Wash., DC, 40 pp.